2008 IEEE International Conference on
Robotics and Automation
Pasadena, CA, USA, May 19-23, 2008

Robotic Airship Trajectory Tracking Control Using a Backstepping Methodology

Filoktimon Repoulias and Evangelos Papadopoulos, *Senior Member, IEEE*

***Abstract*—This paper considers the design of a novel closed-loop trajectory tracking controller for an underactuated robotic airship having 6 degrees of freedom (DOF) and 3 controls, on forward, yaw and pitch motions using two side thrusters. A backstepping methodology is adopted as a design tool, since it is suitable for the cascaded nature of the vehicle dynamics. It also offers design flexibility and robustness against parametric uncertainties which are often encountered in aerodynamic modeling and air stream disturbances. Indeed, in our simulations we assume a 10% error in all dynamic parameters and yet the controller performs position, orientation, linear and angular velocities tracking successfully. We also impose an additional air stream disturbance and the controller corrects the vehicle's trajectory successfully too.**

I. Introduction

ROBOTIC (autonomous) airships [1], see Fig. 1, are employed in various missions such as observation of urban areas or battlefields, in fire detection, rescue, science, and even in planetary exploration [2]. They also present a useful experimental platform for inertial navigation, positioning, and visual sensors [3], and as testbeds for complex control algorithms since almost always such vehicles are underactuated, i.e., they have more DOF than control inputs. Although robotic airships have some advantages against the rest of the autonomous air vehicles at low speeds and low altitude applications [4], they too present a challenging control problem: underactuation imposes non-integrable acceleration constraints. Furthermore, their kinematic and dynamic models are highly nonlinear and coupled [4], [5], making control design a hard task. Underactuation rules out the use of trivial control schemes e.g. full state-feedback linearization [6], and the complex (aero)dynamics excludes designs based solely on kinematics.

During many missions, robotic airships must track an inertial trajectory (a space curve with a specified timing law). This requires the design of control laws that guide and keep the vehicle on the trajectory regardless of external disturbances, modeling errors etc.

Several researchers have addressed the issues of dynamic modeling, hovering, path following, and testing sensors for robotic airships. In [3], a hovering controller using visual servoing for an airship in monitoring tasks was designed. In [4], the physics of airship operation, along with its dynamic model for control design purposes, were presented. In [5], dynamic modeling of indoor airships was presented. In [7], a trajectory tracking controller was designed. In that work, the desired trajectories were constrained to be trimming, i.e., of constant linear and angular velocities. The dynamic model was supposed to be known accurately in control design and velocity errors response were not presented.

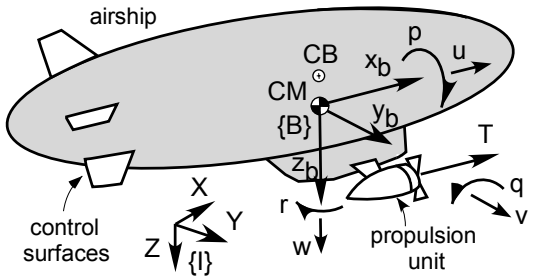

Figure 1. The robotic airship with the controls and motion variables.

The present work was inspired by the similarity of dynamic models and the control actuation of robotic airships and Autonomous Underwater Vehicles (AUVs) [4], [8], and our previous work [9]-[12]: In [9], the combined problem of trajectory planning and tracking control for an underactuated AUV in plane motion was studied. This was the first work in the control literature where trajectory planning, based on the AUV dynamics, was presented. In [10], tracking was designed for trajectories with time-varying velocities where parametric inaccuracies were considered. In [11], we designed a novel, trajectory tracking controller for a six DOF AUV, guided by one propeller and moving surfaces. Simulations showed robustness in dynamic parameters' errors. In [12], we planned dynamically feasible trajectories for an underactuated robotic airship moving in 3D, also a new result. Trajectory planning generates desired variables consistent with vehicle dynamics, thus alleviating a controller in its tracking efforts.

In the present paper we design a novel, closed-loop, trajectory-tracking controller that stabilizes the errors of position, orientation, linear and angular velocities, in a small neighborhood around zero for a robotic airship in 3D motion, having only three controls. Backstepping is used as it suits the cascaded nature of the vehicle dynamics. It also offers design flexibility and robustness in parametric uncertainties and external disturbances. To the best of the authors' knowledge, this is a first work in the robotics control literature where successful tracking results are

Manuscript received September 14, 2008

F. Repoulias is with the National Technical University of Athens (NTUA), Greece (e-mail: firepoul@central.ntua.gr).

E. Papadopoulos is with the National Technical University of Athens (NTUA), Greece (corresponding author, phone: +(30) 210-772-1440; fax: +(30) 210-772-1455; e-mail: egpapado@central.ntua.gr).

presented in full 6 DOF. Moreover, these results were obtained with significant dynamic parametric errors of 10%, in the controller and with an air stream disturbance such as those encountered during flight.

II. Airship Dynamics and Kinematics

In this section, the kinematic and dynamic equations for a robotic airship moving in 3D space are presented.

To describe the kinematics, two reference frames are employed, the inertial reference frame $\{I\}$ and a body-fixed frame $\{B\}$, see Fig. 1. As shown, the origin of $\{B\}$ frame coincides with the airship center of mass (CM) while the center of buoyancy (CB) is on the negative z_b body axis for static stability. The general motion of the airship in 6 DOF can be described by the following vectors:

$$\begin{aligned} &\boldsymbol{\eta}=[\boldsymbol{\eta}_1^T,\boldsymbol{\eta}_2^T]^T;\quad \boldsymbol{\eta}_1=[x,y,z]^T;\quad \boldsymbol{\eta}_2=[\phi,\theta,\psi]^T;\\ &\mathbf{v}=[\mathbf{v}_1^T,\mathbf{v}_2^T]^T;\quad \mathbf{v}_1=[u,\upsilon,w]^T;\quad \mathbf{v}_2=[p,q,r]^T; \end{aligned} \tag{1}$$

In (1), $\boldsymbol{\eta}_1$ denotes the inertial position of the CM and $\boldsymbol{\eta}_2$ the orientation of $\{B\}$ –using Euler angles– with respect to (wrt) the $\{I\}$ frame. Vector $\mathbf{v}_1$ denotes the linear velocity of the CM and $\mathbf{v}_2$ the angular velocity of $\{B\}$ wrt to $\{I\}$ frame, both expressed in $\{B\}$ frame. For the representation of rotations, we use the $x-y-z$ (roll-pitch-yaw) convention defined in terms of Euler angles. Hence, the velocity transformation between $\{B\}$ and frames $\{I\}$ is

$$\dot{\boldsymbol{\eta}}_1=\mathbf{J}_1(\boldsymbol{\eta}_2)\mathbf{v}_1 \tag{2}$$

where,

$$\mathbf{J}_1(\boldsymbol{\eta}_2)=\begin{bmatrix} c\psi c\theta & -s\psi c\phi+c\psi s\theta s\phi & s\psi s\phi+c\psi c\phi s\theta \\ s\psi c\theta & c\psi c\phi+s\phi s\theta s\psi & -c\psi s\phi+s\theta s\psi c\phi \\ -s\theta & c\theta s\phi & c\theta c\phi \end{bmatrix} \tag{3}$$

The body-fixed angular velocities and the time rate of the Euler angles are related through

$$\dot{\boldsymbol{\eta}}_2=\mathbf{J}_2(\boldsymbol{\eta}_2)\mathbf{v}_2 \tag{4}$$

where,

$$\mathbf{J}_2(\boldsymbol{\eta}_2)=\begin{bmatrix} 1 & s\phi t\theta & c\phi t\theta \\ 0 & c\phi & -s\phi \\ 0 & s\phi/c\theta & c\phi/c\theta \end{bmatrix} \tag{5}$$

where $s\cdot=\sin(\cdot)$, $c\cdot=\cos(\cdot)$, $t\cdot=\tan(\cdot)$.

The dynamic model of the airship used in the paper is taken from [4] and [7]. It is a simplified model developed for control design tasks capturing the main dynamical characteristics of a robotic airship in 3D motion, see Fig. 1. Modeling inaccuracies can be treated as small and bounded disturbances that along with air disturbances can be compensated for by a robust closed-loop tracking controller. The vehicle is underactuated, i.e., it has less control inputs than the number of DOF. Regarding the means of propulsion and actuation the following features are used:

Aerodynamic control surfaces like rudders and elevators to control yaw and pitch motions respectively, Fig. 1.

Vectored thrust, meaning the rotation of the propulsion units about an axis parallel to the body–y_b axis providing thrust in the direction required. In this way, pitch torque control is achieved, Fig. 2a. Yaw is controlled using different thrust magnitudes of the side propellers causing a moment about the z_b body axis, Fig. 2b.

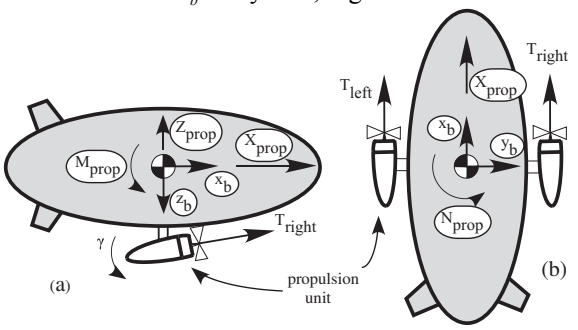

Figure 2. (a) Rotation of the trust by an angle γ for surge force and pitch torque control. (b) Yaw torque control using differential thrust.

Bow and/or stern thrusters are also used for landing and docking operations.

Below a certain speed limit, control surfaces are not effective. Then, ascending or descending is realized by vectoring the thrust down or up, and heading change by using differential thrust in the port and starboard propellers.

In the following equations of motion, the three control variables are X_{prop} for surge propulsion, M_{prop} for pitch torque, and N_{prop} for yaw torque, [4]. These terms are functions of the geometrical arrangement of the propulsive units around the body axes, Fig. 2.

$$m_{11}\dot{u}=m_{22}\upsilon r-m_{33}wq+X_u u+(B-mg)\mathrm{s}\theta+X_{prop} \tag{6a}$$

$$m_{22}\dot{\upsilon}=m_{33}wp-m_{11}ur+Y_\upsilon\upsilon+(mg-B)c\theta s\phi \tag{6b}$$

$$m_{33}\dot{w}=m_{11}uq-m_{22}\upsilon p+Z_w w+(mg-B)c\theta c\phi \tag{6c}$$

$$I_{11}\dot{p}=(I_{22}-I_{33})qr+(m_{22}-m_{33})\upsilon w+K_p p+z_{CB}c\theta s\phi B \tag{6d}$$

$$I_{22}\dot{q}=(I_{33}-I_{11})pr+(m_{33}-m_{11})uw+M_q q+z_{CB}s\theta B+M_{prop} \tag{6e}$$

$$I_{33}\dot{r}=(I_{11}-I_{22})pq+(m_{11}-m_{22})u\upsilon+N_r r+N_{prop} \tag{6f}$$

A brief explanation and the values in SI units, used for the simulations of the various terms in (6), follow: $m=9.07$ is the vehicle's mass and $B=72.2$ is the buoyancy force acting on the CB; $z_{CB}=-0.041$ is the $z-$ coordinate of the CB; $m_{11}=m+X_{\dot{u}}$, $m_{22}=m+Y_{\dot{\upsilon}}$, $m_{33}=m+Z_{\dot{w}}$ are the combined mass and added mass terms, where $X_{\dot{u}}=1.13$, $Y_{\dot{\upsilon}}=7.25$, $Z_{\dot{w}}=7.25$; $I_{11}=I_x+K_{\dot{p}}$, $I_{22}=I_y+M_{\dot{q}}$, $I_{33}=I_z+N_{\dot{r}}$ are the combined mass and added moments of inertia terms, where $I_x=2.19$, $K_{\dot{p}}=0$, $I_y=18.85$, $M_{\dot{q}}=8.87$, $I_z=18.76$, $N_{\dot{r}}=8.87$; $X_u=$ $Y_\upsilon=$ $Z_w=$ $K_p=$ $M_q=$ $N_r=-10$ are the drag, force and moment terms. The system is unactuated in sway υ, heave w, and roll p motions.

III. Trajectory Tracking Control Design

In this section, the tracking control design is presented. Bounded reference velocities and $u\neq 0$ are assumed.

A. Reference Variables

The reference 6 DOF trajectory to be tracked by the

airship is generated by a trajectory planning algorithm developed in [12]. We briefly describe this methodology.

Let a smooth 3D trajectory to be followed by the CM of the airship be given by its inertial coordinates x_R, y_R, and z_R. "R" denotes a reference (desired) variable. Associating the Frenet frame to every point of the curve, we also derive a trajectory-associated orientation. This orientation is not the reference one since the $\{B\}$ frame, during CM tracking of the reference path, undergoes a further rotation wrt Frenet frame due to the inherent dynamics. This rotation is described by the angles of attack and sideslip which are functions of the linear velocities. Hence, we also derive the reference angles ϕ_R, θ_R, and ψ_R. The angular velocities p_R, q_R, and r_R are then obtained by differentiation and the fact that the angular velocity of the $\{B\}$ wrt $\{I\}$ is the sum of the angular velocity of the $\{B\}$ wrt Frenet frame and the angular velocity of the Frenet frame wrt $\{I\}$. The linear velocities u_R, υ_R, and w_R are obtained by the equality of the total airship velocity and the trajectory velocity, and the integration of the unactuated equations (6b) and (6c).

We conclude that this planning methodology provides the full, 6 DOF trajectory, consistent with airship's dynamics.

B. Error Dynamics Formulation

We define the tracking errors as

$$\begin{aligned} &u_e = u - u_R,\ \upsilon_e = \upsilon - \upsilon_R,\ w_e = w - w_R,\\ &p_e = p - p_R,\ q_e = q - q_R,\ r_e = r - r_R,\\ &x_e = x - x_R,\ y_e = y - y_R,\ z_e = z - z_R,\\ &\phi_e = \phi - \phi_R,\ \theta_e = \theta - \theta_R,\ \psi_e = \psi - \psi_R \end{aligned} \tag{7}$$

From (2) and (4) it follows that,

$$\dot{\boldsymbol{\eta}}_{1R} = \mathbf{J}_1(\boldsymbol{\eta}_{2R})\mathbf{v}_{1R} \tag{8a}$$

$$\dot{\boldsymbol{\eta}}_{2R} = \mathbf{J}_2(\boldsymbol{\eta}_{2R})\mathbf{v}_{2R} \tag{8b}$$

Then, the kinematics tracking errors are written as

$$\dot{\boldsymbol{\eta}}_{1e} = \mathbf{J}_1(\boldsymbol{\eta}_2)\mathbf{v}_1 - \mathbf{J}_1(\boldsymbol{\eta}_{2R})\mathbf{v}_{1R} \tag{9a}$$

$$\dot{\boldsymbol{\eta}}_{2e} = \mathbf{J}_2(\boldsymbol{\eta}_2)\mathbf{v}_2 - \mathbf{J}_2(\boldsymbol{\eta}_{2R})\mathbf{v}_{2R} \tag{9b}$$

Substituting in these $\mathbf{v}_1 = \mathbf{v}_{1e} + \mathbf{v}_{1R}$, $\mathbf{v}_2 = \mathbf{v}_{2e} + \mathbf{v}_{2R}$, yields

$$\dot{\boldsymbol{\eta}}_{1e} = \mathbf{J}_1(\boldsymbol{\eta}_2)\mathbf{v}_{1e} + \boldsymbol{\mu}_1 \tag{10a}$$

$$\dot{\boldsymbol{\eta}}_{2e} = \mathbf{J}_2(\boldsymbol{\eta}_2)\mathbf{v}_{2e} + \boldsymbol{\mu}_2 \tag{10b}$$

where terms $\boldsymbol{\mu}_1$ and $\boldsymbol{\mu}_2$ are given by,

$$\boldsymbol{\mu}_1 = [\mathbf{J}_1(\boldsymbol{\eta}_2) - \mathbf{J}_1(\boldsymbol{\eta}_{2R})]\mathbf{v}_{1R} \tag{11a}$$

$$\boldsymbol{\mu}_2 = [\mathbf{J}_2(\boldsymbol{\eta}_2) - \mathbf{J}_2(\boldsymbol{\eta}_{2R})]\mathbf{v}_{2R} \tag{11b}$$

and are both treated as bounded time-varying disturbances.

Considering the dynamics, and setting

$$X_{prop} = m_{33}wq - m_{22}\upsilon r - X_u u - (B - mg)s\theta + m_{11}\tau_u \tag{12}$$

$$M_{prop} = (I_{11} - I_{33})pr + (m_{11} - m_{33})uw - M_q q - z_{CB}s\theta B + I_{22}\tau_q \tag{13}$$

$$N_{prop} = (I_{22} - I_{11})pq + (m_{22} - m_{11})u\upsilon - N_r r + I_{33}\tau_r \tag{14}$$

we obtain the following partially linearized system:

$$\dot{u}_e = -\dot{u}_R + \tau_u \tag{15a}$$

$$\dot{\upsilon}_e = -(m_{11}/m_{22})ur_e + \varepsilon_\upsilon \tag{15b}$$

$$\dot{w}_e = (m_{11}/m_{33})uq_e + \varepsilon_w \tag{15c}$$

$$\dot{p}_e = (K_p/I_{11})p_e + \varepsilon_p \tag{15d}$$

$$\dot{q}_e = -\dot{q}_R + \tau_q \tag{15e}$$

$$\dot{r}_e = -\dot{r}_R + \tau_r \tag{15f}$$

where τ_u, τ_q, and τ_r are auxiliary controls and ε_υ, ε_w, and ε_p are functions of the errors and reference variables.

C. Error Dynamics Stabilization

We firstly make a few observations regarding the control design: considering (15), we note that the controlled velocities are u_e, q_e, and r_e, using τ_u, τ_q, and τ_r respectively. In order to control the position (10a) and orientation (10b), we use in a first step, as virtual controls, the velocities u_e, υ_e, w_e, and q_e, r_e, respectively. Although υ_e, and w_e are not directly controlled, we exploit the couplings ur_e and uq_e –and the natural for tracking nonzero surge velocity assumption– with the controlled variables q_e and r_e for control; p_e is not controlled either, but exploiting the stabilizing negative term (K_p/I_{11}) in (15d) and the decrease of ε_p when the rest of the system is stabilized, the former is also stabilized around zero.

In the sequel, we proceed to the design of a control law for the underactuated system of (10a), (10b), and (15a)-(15f) employing backstepping and nonlinear damping.

Step 1. Considering (10a), we take as virtual control the vector $\mathbf{v}_{1e} = [u_e, \upsilon_e, w_e]^T$, we ignore for now $\boldsymbol{\mu}_1$, and set

$$\mathbf{v}_{1e,des} = -\mathbf{J}_1^T(\mathbf{K} + \mathbf{K}_1)\boldsymbol{\eta}_{1e} \triangleq \boldsymbol{\alpha}_{\mathbf{v}1} = [\alpha_u, \alpha_\upsilon, \alpha_w]^T \tag{16}$$

where $\mathbf{K} \triangleq diag(k,k,k)$ and $\mathbf{K}_1 \triangleq diag(k_1,k_1,k_1)$ are positive definite gain matrices. The components of $\boldsymbol{\alpha}_{\mathbf{v}1}$ are not true controls. Hence, we introduce appropriate error variables:

$$\mathbf{z}_u = [z_u, z_\upsilon, z_w]^T \triangleq [u_e - \alpha_u, \upsilon_e - \alpha_\upsilon, w_e - \alpha_w]^T \tag{17}$$

Then, the controlled subsystem so far becomes:

$$\dot{\boldsymbol{\eta}}_{1e} = \mathbf{J}_1[\boldsymbol{\alpha}_{\mathbf{v}1} + \mathbf{z}_u] + \boldsymbol{\mu}_1 \tag{18}$$

To stabilize z_u using τ_u and the position $\boldsymbol{\eta}_{1e}$, we choose

$$V_1 = (\boldsymbol{\eta}_{1e}^T\boldsymbol{\eta}_{1e} + z_u^2)/2 \tag{19}$$

Then, its time derivative becomes

$$\begin{aligned} \dot{V}_1 = &-\boldsymbol{\eta}_{1e}^T(\mathbf{K} + \mathbf{K}_1)\boldsymbol{\eta}_{1e} + \boldsymbol{\eta}_{1e}^T\boldsymbol{\mu}_1 + z_w[z_e c\phi c\theta + y_e(c\phi s\psi s\theta\\ &- c\psi s\phi) + x_e(s\phi s\psi + c\phi c\psi s\theta)] + z_\upsilon[z_e c\theta s\phi\\ &+ y_e(s\phi s\psi s\theta + c\phi c\psi) + x_e(c\psi s\phi s\theta - c\phi s\psi)]\\ &+ z_u[\tau_u - \dot{u}_R - \dot{\alpha}_u + x_e c\psi c\theta + y_e c\theta s\psi - z_e s\theta] \end{aligned} \tag{20}$$

Young's inequality [6], nonlinear damping [13], setting

$$\tau_u = \dot{u}_R - c_{zu1}z_u - c_{zu3}z_u^3 + \dot{\alpha}_u - x_e c\psi c\theta - y_e c\theta s\psi + z_e s\theta] \tag{21}$$

and after some straightforward manipulations, (20) becomes

$$\begin{aligned} \dot{V}_1 \le &-\boldsymbol{\eta}_{1e}^T(\mathbf{K} - \boldsymbol{\Lambda})\boldsymbol{\eta}_{1e} + [\|\boldsymbol{\mu}_1\|^2/4k_1] + \gamma_1\\ &+ [(z_\upsilon^2 + z_w^2)/4\lambda] - [c_{zu1} - (1/4\lambda)]z_u^2 - c_{zu3}z_u^4 \end{aligned} \tag{22}$$

where $\boldsymbol{\Lambda} \triangleq diag(\lambda,\lambda,\lambda)$ is a positive definite gain matrix, $k > \lambda$, and c_{zu1}, c_{zu3} are positive constants with $c_{zu1} > 1/4\lambda$. Also, γ_1 is a function position errors.

Step 2. Considering the subsystems that are controlled by r_e and q_e, i.e., the rotational kinematics and the errors z_υ and z_w we have: for (10b), we take as virtual controls the

vector $\mathbf{v}_{2e}=[p_e,q_e,r_e]^T$ and ignore for now the term $\boldsymbol{\mu}_2$. We choose the first part of the desired expressions for these as

$$\mathbf{v}_{2e,des}=-\mathbf{J}_2^{-1}(\mathbf{K}_2+\mathbf{K}_3)\boldsymbol{\eta}_{2e}\triangleq\boldsymbol{\alpha}_{v2}=[\alpha_p,\alpha_{q1},\alpha_{r1}]^T \quad (23)$$

where $\mathbf{K}_2\triangleq diag(k_2,k_2,k_2)$ and $\mathbf{K}_3\triangleq diag(k_3,k_3,k_3)$ are positive definite gain matrices. The inversion of $\mathbf{J}_2$ results in the singular point $\theta=\pm\pi/2$, but the vehicle will not operate near this point. Next, for the dynamics

$$\dot{z}_\upsilon=-(m_{11}/m_{22})ur_e+\varepsilon_\upsilon-\dot{\alpha}_\upsilon \quad (24)$$

$$\dot{z}_w=(m_{11}/m_{33})uq_e+\varepsilon_w-\dot{\alpha}_w \quad (25)$$

we choose

$$q_{e,wdes}=-c_q uz_w\triangleq\alpha_{q2} \quad (26)$$

$$r_{e,\upsilon des}=c_r uz_\upsilon\triangleq\alpha_{r2} \quad (27)$$

where c_q and c_r are positive constants. Considering (23),

$$\alpha_q=\alpha_{q1}+\alpha_{q2} \quad (28)$$

$$\alpha_r=\alpha_{r1}+\alpha_{r2} \quad (29)$$

So far, the controlled subsystem of the rotational kinematics and the errors z_υ and z_w is transformed as

$$\dot{\boldsymbol{\eta}}_{2e}=-(\mathbf{K}_2+\mathbf{K}_3)\boldsymbol{\eta}_{2e}+\boldsymbol{\mu}_2+\mathbf{f}_{\eta 2} \quad (30)$$

$$\dot{z}_\upsilon=-c_r(m_{11}/m_{22})u^2z_\upsilon+f_\upsilon \quad (31)$$

$$\dot{z}_w=-c_q(m_{11}/m_{33})u^2z_w+f_w \quad (32)$$

where $\mathbf{f}_{\eta 2}$, f_υ, and f_w are functions of the states.

In order to stabilize the above subsystem, we choose

$$V_2=(\boldsymbol{\eta}_{1e}^T\boldsymbol{\eta}_{1e}+\boldsymbol{\eta}_{2e}^T\boldsymbol{\eta}_{2e}+z_u^2+z_\upsilon^2+z_w^2)/2 \quad (33)$$

Taking into account (22), and using nonlinear damping, its time derivative becomes

$$\begin{aligned}\dot{V}_2\le&-\boldsymbol{\eta}_{1e}^T(\mathbf{K}-\boldsymbol{\Lambda})\boldsymbol{\eta}_{1e}-\boldsymbol{\eta}_{2e}^T\mathbf{K}_2\boldsymbol{\eta}_{2e}+[\|\boldsymbol{\mu}_1\|^2/4k_1]\\&+\gamma_2-[c_{zu1}-(1/4\lambda)]z_u^2-c_{zu3}z_u^4+[(z_\upsilon^2+z_w^2)/4\lambda]\\&-c_r(m_{11}/m_{22})u^2z_\upsilon^2-c_q(m_{11}/m_{33})u^2z_w^2+[\|\boldsymbol{\mu}_2\|^2/4k_3]\end{aligned} \quad (34)$$

where γ_2 is a function of γ_1, $\mathbf{f}_{\eta 2}$, f_υ, f_w, discussed later.

Step 3. The variables p_e, q_e and r_e are not true controls. Thus, we introduce the errors $z_p\triangleq p_e-\alpha_p$, $z_q\triangleq q_e-\alpha_q$ and $z_r\triangleq r_e-\alpha_r$ in (15d) and in (30)-(32) yielding:

$$\dot{z}_p=(K_p/I_{11})z_p+\varepsilon_{p1} \quad (35)$$

with ε_{p1} function of α_p and ε_p.

$$\dot{z}_\upsilon=-c_r(m_{11}/m_{22})u^2z_\upsilon+(m_{11}/m_{22})uz_r+f_\upsilon \quad (36)$$

$$\dot{z}_w=-c_q(m_{11}/m_{33})u^2z_w+(m_{11}/m_{33})uz_q+f_w \quad (37)$$

$$\dot{\boldsymbol{\eta}}_{2e}=-(\mathbf{K}_2+\mathbf{K}_3)\boldsymbol{\eta}_{2e}+\mathbf{J}_2[z_p,z_q,z_r]^T+\boldsymbol{\mu}_2+\mathbf{f}_{\eta 2} \quad (38)$$

We now choose

$$V_3=(\boldsymbol{\eta}_{1e}^T\boldsymbol{\eta}_{1e}+\boldsymbol{\eta}_{2e}^T\boldsymbol{\eta}_{2e}+z_p^2+z_u^2+z_\upsilon^2+z_w^2+z_q^2+z_r^2)/2 \quad (39)$$

and taking its time derivative we have

$$\begin{aligned}\dot{V}_3\le&-\boldsymbol{\eta}_{1e}^T(\mathbf{K}-\boldsymbol{\Lambda})\boldsymbol{\eta}_{1e}-\boldsymbol{\eta}_{2e}^T\mathbf{K}_2\boldsymbol{\eta}_{2e}+[\|\boldsymbol{\mu}_1\|^2/4k_1]-c_{zu3}z_u^4\\&+(K_p/I_{11})z_p^2+[\|\boldsymbol{\mu}_2\|^2/4k_3]-[c_{zu1}-(1/4\lambda)]z_u^2\\&-c_r(m_{11}/m_{22})u^2z_\upsilon^2-c_q(m_{11}/m_{33})u^2z_w^2+z_r[\tau_r\\&-\dot{r}_R-\dot{\alpha}_r+(m_{11}/m_{22})uz_\upsilon+\psi_e(c\phi/c\theta)-\theta_e s\phi\\&+\phi_e c\phi t\theta]+z_q[\tau_q-\dot{q}_R-\dot{\alpha}_q+(m_{11}/m_{33})uz_w+\theta_e c\phi\\&+\psi_e(s\phi/c\theta)+\phi_e s\phi t\theta]+\gamma_3\end{aligned} \quad (40)$$

where γ_3 is a smooth function of the states. We now set the controls τ_q and τ_r as follows:

$$\begin{aligned}\tau_q=&\dot{q}_R+\dot{\alpha}_q-(m_{11}/m_{33})uz_w-\theta_e c\phi\\&-\psi_e(s\phi/c\theta)-\phi_e s\phi t\theta]-c_{zq1}z_q-c_{zq3}z_q^3\end{aligned} \quad (41)$$

$$\begin{aligned}\tau_r=&\dot{r}_R+\dot{\alpha}_r-(m_{11}/m_{22})uz_\upsilon-\psi_e(c\phi/c\theta)\\&+\theta_e s\phi-\phi_e c\phi t\theta-c_{zr1}z_r-c_{zr3}z_r^3\end{aligned} \quad (42)$$

with c_{zq1}, c_{zq3}, c_{zr1}, c_{zr3} positive constants; (40) becomes

$$\begin{aligned}\dot{V}_3\le&-\boldsymbol{\eta}_{1e}^T(\mathbf{K}-\boldsymbol{\Lambda})\boldsymbol{\eta}_{1e}-\boldsymbol{\eta}_{2e}^T\mathbf{K}_2\boldsymbol{\eta}_{2e}+[\|\boldsymbol{\mu}_1\|^2/4k_1]-c_{zu3}z_u^4\\&+(K_p/I_{11})z_p^2+[\|\boldsymbol{\mu}_2\|^2/4k_3]-[c_{zu1}-(1/4\lambda)]z_u^2\\&-c_r(m_{11}/m_{22})u^2z_\upsilon^2-c_q(m_{11}/m_{33})u^2z_w^2\\&-c_{zr1}z_r^2-c_{zr3}z_r^4-c_{zq1}z_q^2-c_{zq3}z_q^4+\gamma_3\end{aligned} \quad (43)$$

Before proceeding, we make the following assumptions concerning positive terms like $\|\boldsymbol{\mu}_1\|$, and terms with undefined sign, like the terms contained in γ_3.

Assumptions: 1) Each of the time-varying terms (that stem from the reference trajectory) has a constant upper bound (e.g. $0<\|r_R\|\le r_{R,\max}$). This is set during trajectory planning.

2) The uncontrolled velocities have upper bounds, $\|\upsilon_e\|\le\upsilon_{e,\max}$, $\|w_e\|\le w_{e,\max}$, and $\|p_e\|\le p_{e,\max}$, where $\upsilon_{e,\max}$, $w_{e,\max}$, and $p_{e,\max}$ are positive constants. We can think of these bounds as the maximum admissible operating limits ("flight envelope") beyond which a guidance law is needed.

3) The surge velocity has lower and upper bounds, $\|u\|\le u_{\max}$, where $u_{\max}$ is a positive constant, and $u\neq 0$ as already has been stated.

After tedious but straightforward algebraic manipulations of the various terms in (43), and taking into account the above assumptions, we end up with the following:

$$\begin{aligned}\dot{V}_3\le&-\boldsymbol{\eta}_{1e}^T\boldsymbol{\Pi}_1\boldsymbol{\eta}_{1e}-\boldsymbol{\eta}_{2e}^T\boldsymbol{\Pi}_2\boldsymbol{\eta}_{2e}+c_1z_p^2-c_2z_u^2\\&-c_3(u)z_\upsilon^2-c_4(u)z_w^2-c_5z_r^2-c_6z_q^2+c_o\end{aligned} \quad (44)$$

where $\boldsymbol{\Pi}_1\triangleq diag(\pi_1,\pi_1,\pi_1)$ and $\boldsymbol{\Pi}_2\triangleq diag(\pi_2,\pi_2,\pi_2)$ are positive definite gain matrices. The gain c_1 is negative as and the gains $c_3(u)$ and $c_4(u)$ are positive when $u\neq 0$. Also, c_o is a positive constant, which can be made very small using an appropriate combination of the values of the various gains. Now, if we define

$$\mathbf{z}\triangleq[\boldsymbol{\eta}_{1e}^T,\boldsymbol{\eta}_{2e}^T,z_u,z_\upsilon,z_w,z_p,z_q,z_r]^T \quad (45)$$

we find that

$$2V_3=\|\mathbf{z}\|^2 \quad (46)$$

Taking $\xi=\min\{\pi_1,\pi_2,-c_1,c_2,c_3,c_4,c_5,c_6\}$, then

$$\dot{V}_3\le-2\xi V_3+c_o \quad (47)$$

which, by employing the Comparison Lemma [6], yields

$$V_3(t)\le V_3(0)e^{-2\xi t}+(c_o/2\xi) \quad (48)$$

for $t\in[0,t_{final})$. Doing the algebra, we conclude that

$$\|\mathbf{z}(t)\|\le\|\mathbf{z}(0)\|e^{-\xi t}+\sqrt{c_o/\xi},\quad t\in[0,t_{final}) \quad (49)$$

Eq. (49) means that the states of the error dynamics remain in a small, bounded set around zero, which can be reduced using an appropriate combination of the controller

gains. At this result we arrived using (12), (13), and (14), along with (21), (41), and (42).

IV. Simulation Results

In this section, we present simulation results to illustrate the effectiveness of the designed controller. The reference helix CM trajectory is described by the following equations

$$x_R = 30\cos(0.01t) \text{ m} \quad (50a)$$

$$y_R = 30\sin(0.01t) \text{ m} \quad (50b)$$

$$z_R = 0.025t \text{ m} \quad (50c)$$

The rest of the reference variables, computed as in [12], are $u_R = 0.3$, $\upsilon_R = 3.6\times10^{-3}$, $w_R \cong 10^{-5}$ in m/s, $p_R = -8.3\times10^{-4}$, $q_R \cong 10^{-6}$, $r_R = 10^{-2}$ in rad/s, and $\phi_R = 10^{-3}$, $\theta_R = -0.083$, $\psi_R = -0.01t$ in rad. The initial errors are set as $\|x_e\|=0.4$, $\|y_e\|=0.33$, $\|z_e\|=0.25$ in m, $\|\phi_e\|=\|\theta_e\|=\|\psi_e\|=1$ deg, $\|u_e\|=0.1$, $\|\upsilon_e\|=0.03$, $\|w_e\|=0$ in m/s, and $\|p_e\|=10^{-3}$, $\|q_e\|=\|r_e\|=0$ in rad/s. The dynamic model used is that of (6). However, in order to investigate the robustness of the controller, we introduced errors of the order of $\pm10\%$ in all dynamic parameters used in the control law. The simulations were obtained with controller gains chosen as: $k = k_2 = c_{zu3} = 4$, $k_1 = c_{zq1} = c_{zq3} = c_{zu1} = 3$, $c_{zr1} = c_{zr3} = 1$, $c_r = 0.1$, and $c_q = 0.5$.

In Fig. 3, the reference and the resulting trajectory of the CM of the airship in the inertial space are displayed. We see the fast convergence of the CM trajectory to the desired one.

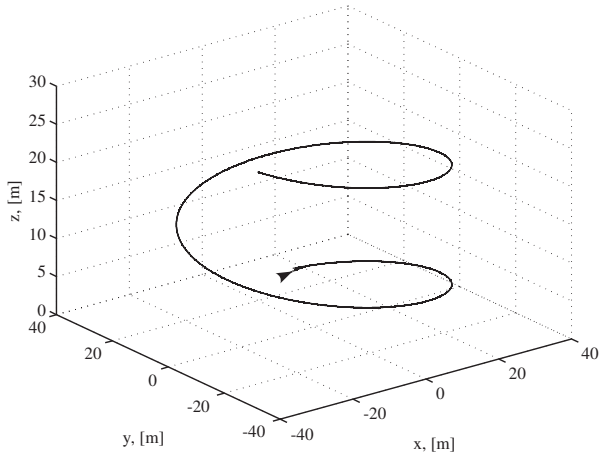

Figure 3. The actual and the reference 3D space path.

Fig. 4 shows the control force X_{prop} and torques M_{prop}, and N_{prop}. The errors in linear velocities which converge after 20 s, are depicted in Fig. 5(a, b, c, d, e, and f). In Fig. 6(a, b, c, d, e, and f), the errors in the angular velocities which converge after 25 s are shown. In Fig. 7(a, b, c, d, e, and f), we can see that the inertial position errors converge in about 20 s, in a small neighborhood of zero, of the order of 2 mm, and slowly oscillate within. In Fig. 8(a, b, c, d, e, and f), we see the Euler angles errors to converge smoothly to a neighborhood of zero of the order of 0.3 deg, in about 25 s.

We then conduct a simulation imposing a steady air stream disturbance of 1.5 m/s in the inertial x direction keeping the parametric uncertainties. We can see in Fig. 9, that the controller counteracts the disturbance and the airship follows the desired path.

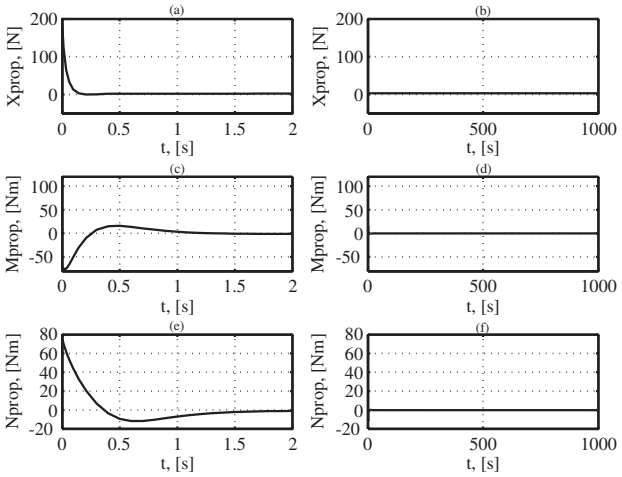

Figure 4. Control force and torques. (a), (c), (e) First 2 s. (b), (d), (f) 1000 s.

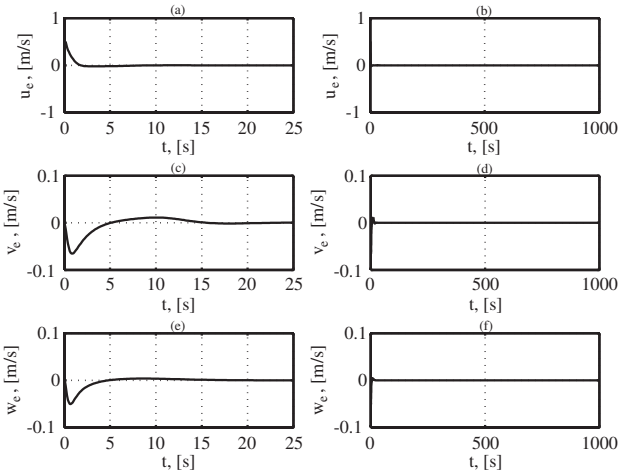

Figure 5. Linear velocities tracking errors. (a), (c), (e) First 25 s. (b), (d), (f) 1000 s.

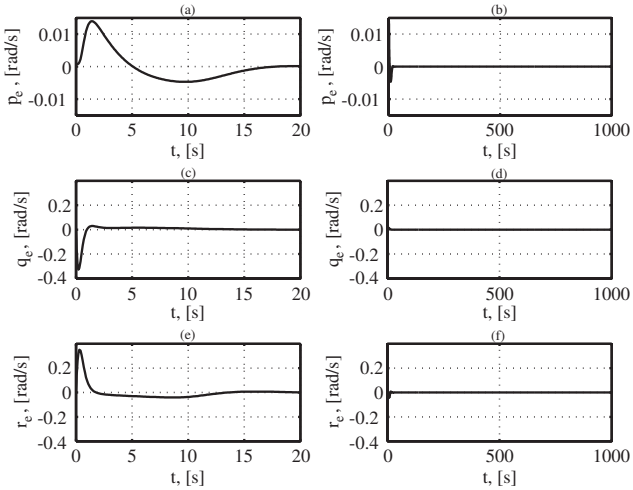

Figure 6. Angular velocities errors. (a), (c), (e) First 20 s. (b), (d), (f) 1000 s.

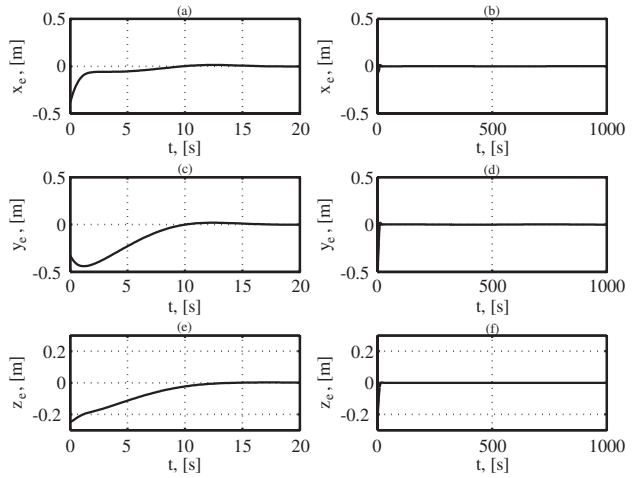

Figure 7. Inertial position tracking errors. (a), (c), (e) First 20 s. (b), (d), (f) 1000 s.

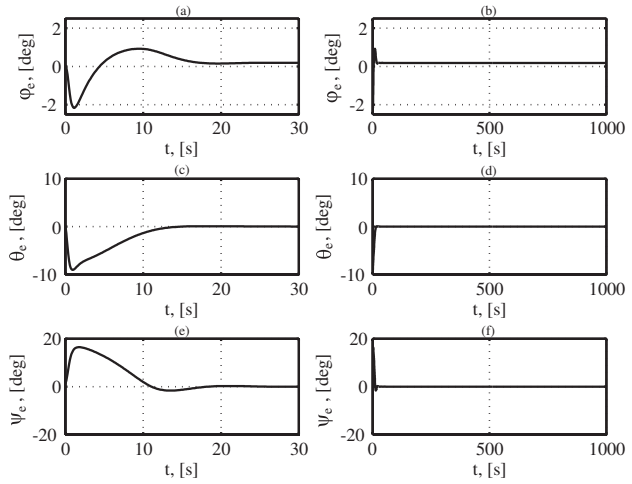

Figure 8. Euler angles tracking errors. (a), (c), (e) First 30 s. (b), (d), (f) 1000 s.

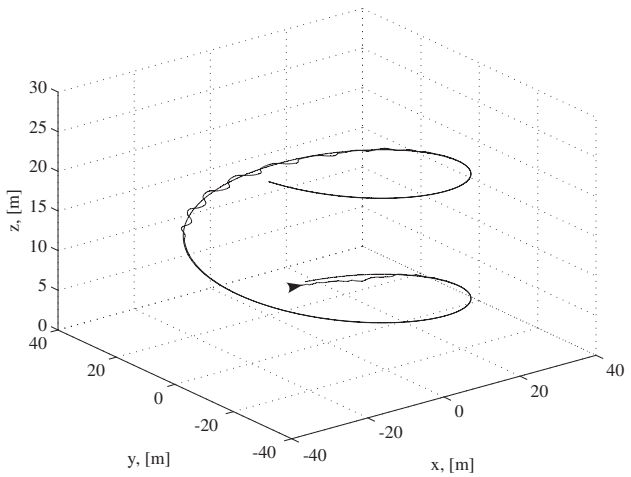

Figure 9. The actual and the reference path in the presence of air stream.

V. CONCLUSIONS

In this paper, we presented a novel closed-loop tracking controller for an underactuated robotic airship, in 3D space, having only 3 control inputs. We adopted backstepping as our design methodology, as it offers flexibility and robustness against parametric uncertainties and environmental disturbances, which is inherent in Lyapunov techniques. To the best of the authors' knowledge, this is a first work in the robotics control literature, where successful tracking results are presented in position, orientation and linear and angular velocities, i.e., in full 6 DOF. Moreover, these results were obtained with significant dynamic parametric errors of 10%, in the controller and with an air stream disturbance such as those encountered during flight.

For future work, we intend to present results of the application of the developed tracking controller in the case of trajectories with time-varying velocities. We currently study the derivation of an analytical expression between the gains and the maximum errors of the unactuated variables and as well as between the gains and the neighborhood of zero that the tracking errors converge.

REFERENCES

[1] G. A. Khoury and J. D. Gillet, *Airship Technology.* Cambridge University Press, 1999.

[2] A. Elfes, et. al., "Robotic airships for exploration of planetary bodies with an atmosphere: autonomy challenges," *Autonomous Robots,* vol. 14, pp. 147-164, 2003.

[3] J. R. Azinheira, et. al., "Visual servo control for the hovering of an outdoor robotic airship," *IEEE International Conference on Robotics and Automation,* Washington DC, USA, May 2002.

[4] S. B. V. Gomes and J. J. Ramos, "Airship dynamic modeling for autonomous operation," *IEEE International Conference on Robotics and Automation,* Leuven, Belgium, May 1998.

[5] J. C. Zufferey, et. al., "Flying over the reality gap: Form simulated to real indoor airships," *Autonomous Robots,* vol. 21, pp. 243-254, 2006.

[6] H. K. Khalil, *Nonlinear Systems,* 2nd ed, Prentice Hall, Upper Saddle River, 1996.

[7] L. Beji and A Abichou,, "Tracking control of trim trajectories of a blimp for ascent and descent flight maneuvers," in *International Journal of Control,* vol. 78, pp. 706-719, July 2005.

[8] T. I. Fossen, *Guidance and Control of Ocean Vehicles,* New York: Wiley, 1994.

[9] F. Repoulias, and E. Papadopoulos, "Trajectory planning and tracking control design of underactuated AUVs," *Proc. IEEE Int. Conf. on Robotics and Automation (ICRA 2005),* Barcelona, Spain, 2005, pp.1622-1627.

[10] F. Repoulias, and E. Papadopoulos, "Planar trajectory planning and tracking control design for underactuated AUVs," *Ocean Engineering*, vol. 34, No. 11-12, pp 1650-1667, August 2007.

[11] F. Repoulias, and E. Papadopoulos, "Three dimensional trajectory control of underactuated AUVs," *Proc. European Control Conference (ECC 2007),* Kos, Greece, July 2007.

[12] F. Repoulias, and E. Papadopoulos, "Dynamically feasible trajectory and open-loop control design for unmanned airships," *Proc. IEEE Mediterranean Conf. on Control and Automation (MED 2007),* Athens, Greece, June 2007.

[13] M. Krstic, I. Kanellakopoulos, and P. Kokotovic, *Nonlinear and Adaptive Control Design,* New York: Wiley, 1995.